Supporting Information

Importance of selective quenching of the triplet excited state of thermally activated delayed fluorescence (TADF) photosensitizers in redox-photosensitized reactions: case studies on photocatalytic CO_2 reduction

Yusuke Tamaki[*†], Kei Kamogawa[‡], Rei Inoue[§], Paola Ceroni[∥], and Osamu Ishitani*[*‡]*

[†]National Institute of Advanced Industrial Science and Technology (AIST), 4-2-1 Nigatake, Miyaginoku, Sendai, Miyagi 983-8551, Japan.

[‡]Department of Chemistry, Graduate School of Advanced Science and Engineering, Hiroshima University, 1-3-1 Kagamiyama, Higashi-Hiroshima, Hiroshima 739-8526, Japan.

[§]Department of Chemistry, School of Science, Tokyo Institute of Technology, 2-12-1 O-okayama, Meguroku, Tokyo 152-8550, Japan.

[∥]Dipartimento di Chimica "Giacomo Ciamician", Alma Mater Studiorum– Universit`a di Bologna, Via Selmi 2, 40126 Bologna, Italy.

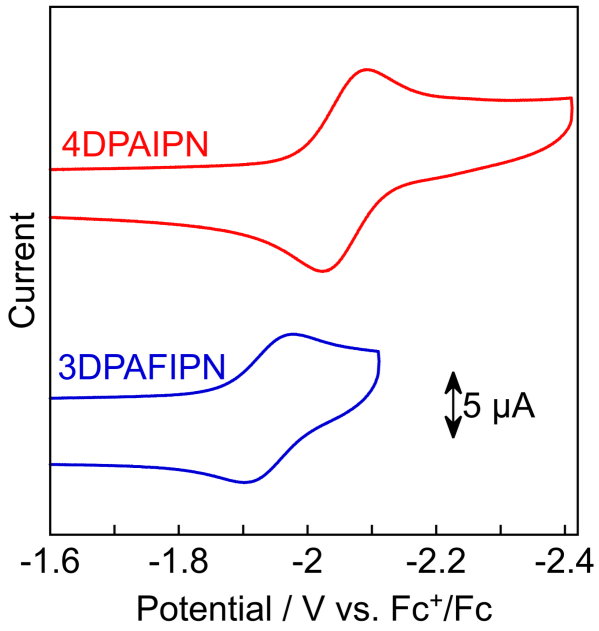

Figure S1. Cyclic voltammograms of **4DPAIPN** (red line) and **3DPAFIPN** (blue line) measured in Ar-saturated DMA containing Et_4NBF_4 (0.1 M) as a supporting electrolyte with a $Ag/AgNO_3$ (10 mM) reference electrode. The Fc^+/Fc redox couple was also measured and taken as the standard. Scan rate was 0.2 $V \cdot s^{-1}$.

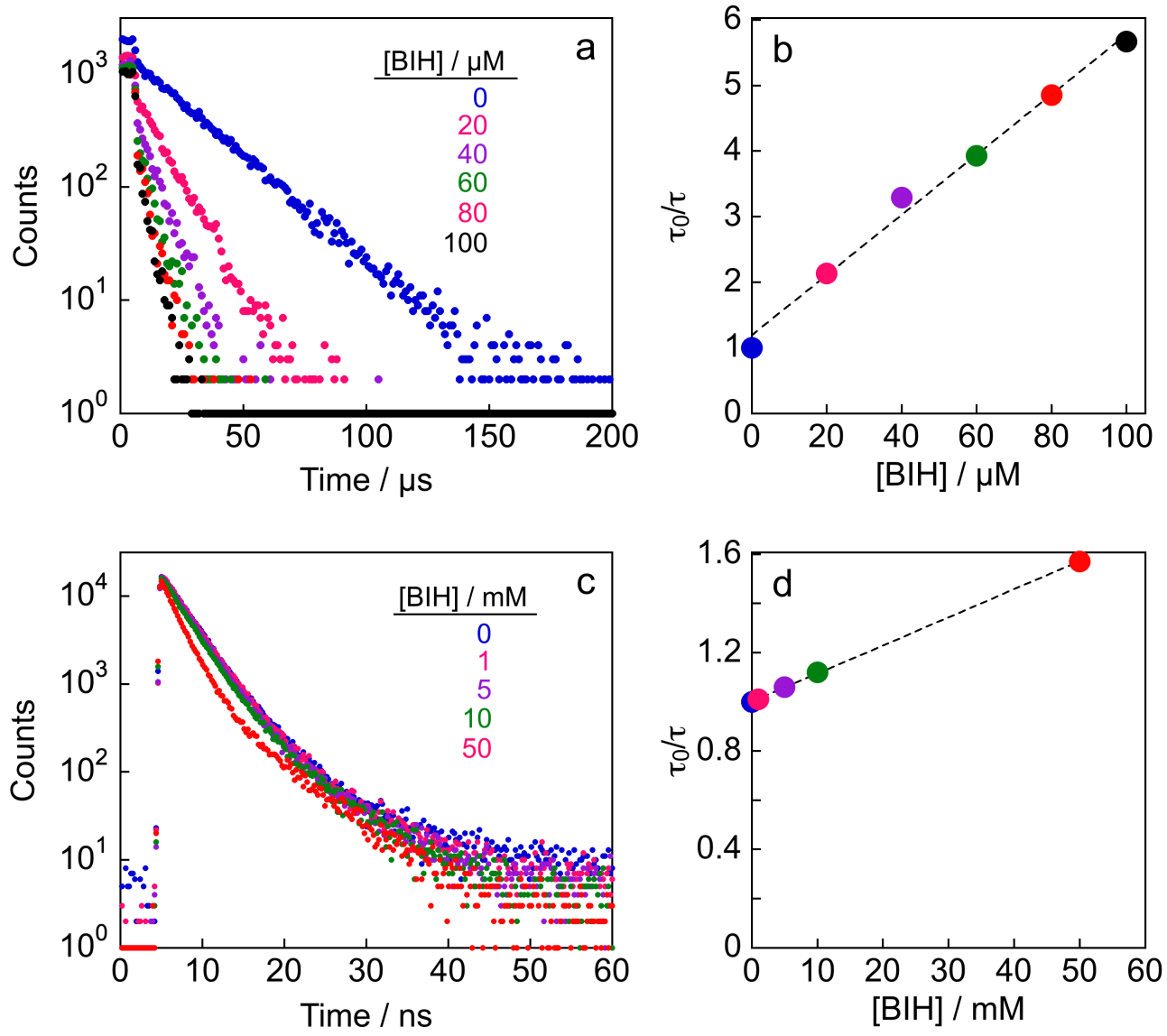

Figure S2. (a),(c) Emission intensity decays (λ_{em} = 530 nm) of **4DPAIPN** in the presence of various concentrations of BIH and (b),(d) the corresponding Stern–Volmer plots. (a),(b) represents the quenching of TADF measured in Ar-saturated DMA–TEOA (1.5 M) upon λ_{ex} = 459 nm. (c),(d) represents the quenching of prompt fluorescence measured in air-equilibrated DMA–TEOA (1.5 M) upon λ_{ex} = 444 nm. Although ^{3}**4DPAIPN*** is quenched by TEOA as well, for determining the quenching rate constants, we can assume that k_q^{TEOA}[TEOA] is constant and this value is included in τ_0 measured in DMA–TEOA (1.5 M). We selected this DMA–TEOA (1.5 M) solution because the properties of solutions (such as viscosity) for measuring the quenching rate constants by BIH should be similar to those in the photocatalytic reactions. These decay curves were carefully remeasured, and we found that the previous reported quenching rate constants[1] are not correct, thus we revised as $^1k_q = 3.6\times10^9$ $M^{-1}s^{-1}$ and $^3k_q^{BIH} = 2.0\times10^9$ $M^{-1}s^{-1}$.

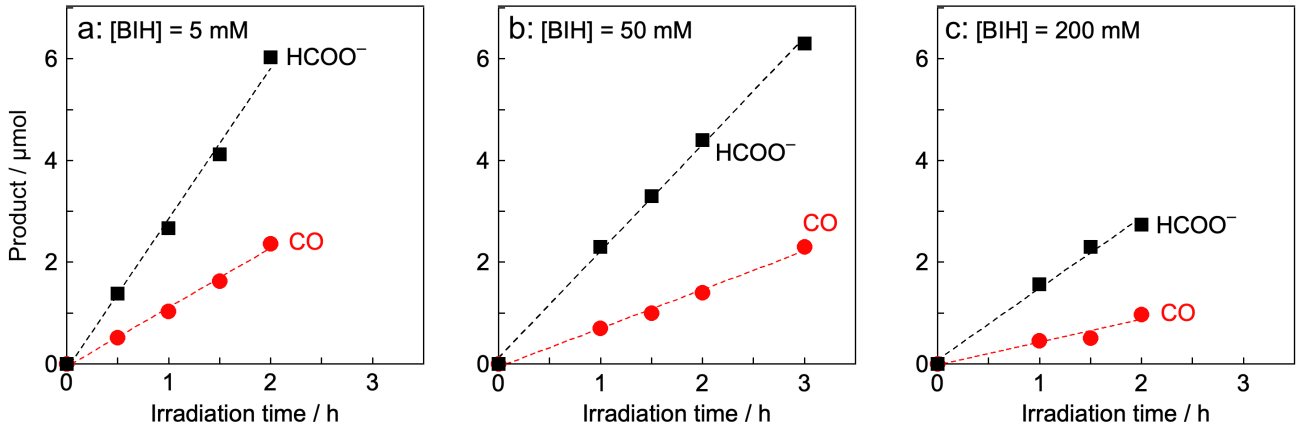

Figure S3. Photocatalytic production of CO (●) and $HCOO^-$ (■) using (a) 5 mM, (b) 50 mM, or (c) 200 mM of BIH: CO_2-saturated DMA solutions (4 mL) containing **4DPAIPN** (50 μM), **Mn** (50 μM), BIH and TEOA (1.5 M) were irradiated at λ_{ex} = 480 nm. Light intensity = 5.0×10^{-9} Einstein·s^{-1}.

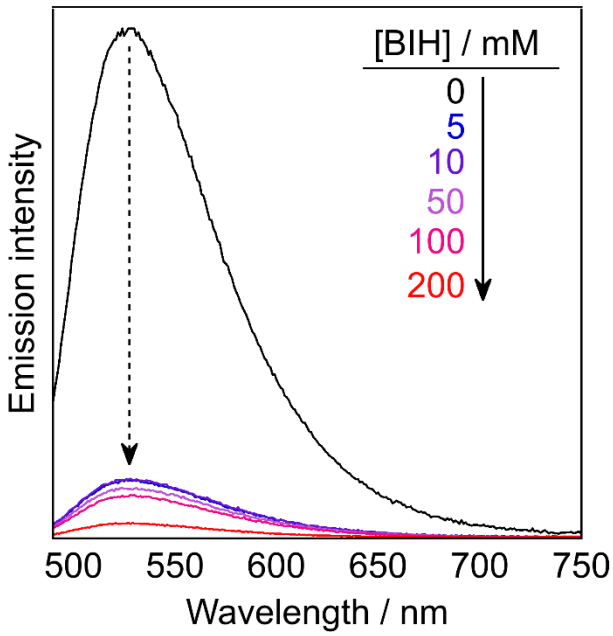

Figure S4. Emission spectra of **4DPAIPN** measured in an Ar-saturated DMA solution ([BIH] = [TEOA] = 0 M) and DMA solution containing TEOA (1.5 M) and various concentrations of BIH (5-200 mM). Excitation wavelength was λ_{ex} = 480 nm.

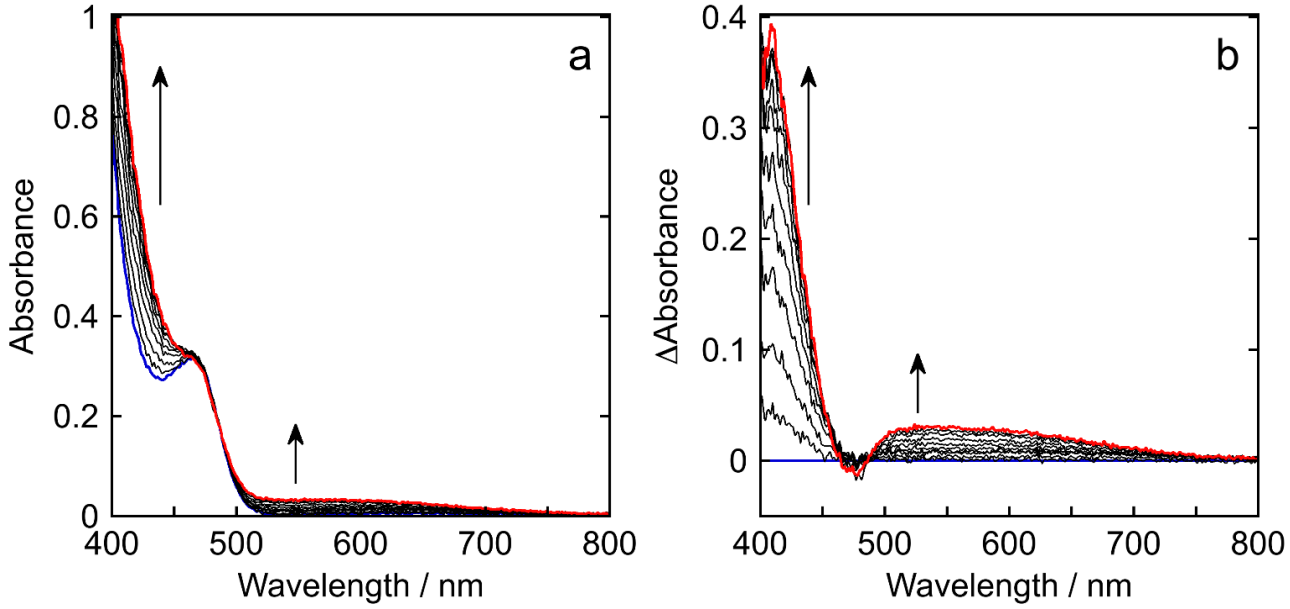

Figure S5. (a) UV-vis absorption spectral change of a CO_2-saturated DMA-TEOA (1.5 M) solution containing **4DPAIPN** (50 μM) and BIH (0.1 M) during irradiation at 480-nm light for 0-300 s at 30-s intervals. (b) Differential spectra between post- and pre-irradiation spectra. The blue and red lines represent the spectra of irradiation for 0 and 300 s, respectively. Light intensity was 2.4×10^{-8} Einstein·s^{-1}.

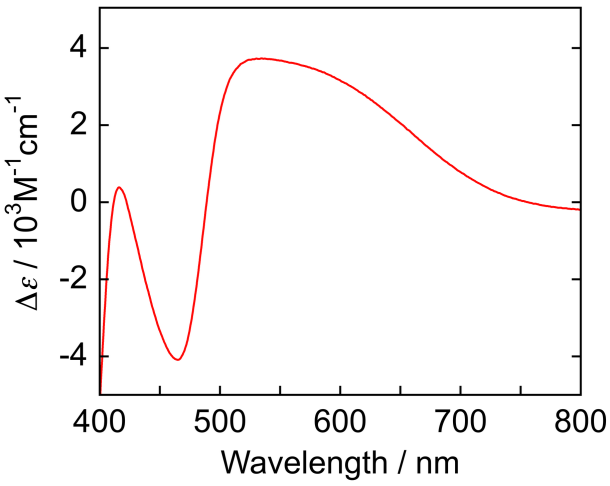

Figure S6. UV-vis absorption spectrum of **4DPAIPN•⁻** in an Ar-saturated DMA solution containing 0.1 M Et_4NBF_4 obtained by the flow electrolysis method

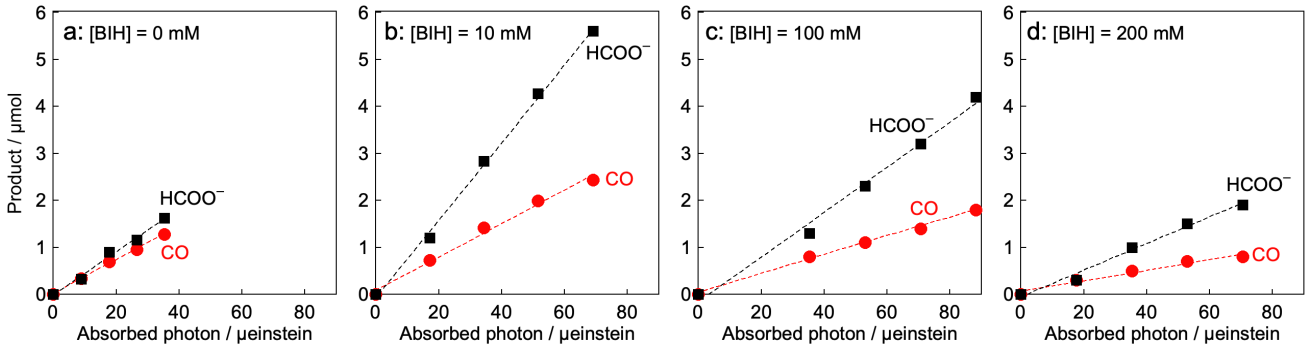

Figure S7. Photocatalytic production of CO (●) and $HCOO^-$ (■) using (a) 0 mM, (b) 10 mM, (c) 100 mM, or (d) 200 mM of BIH: CO_2-saturated DMA solutions (4 mL) containing **3DPAFIPN** (250 μM), **Mn** (50 μM), BIH and TEOA (1.5 M) were irradiated at λ_{ex} = 430 nm. Light intensity = 5.0×10^{-9} Einstein·s^{-1}.

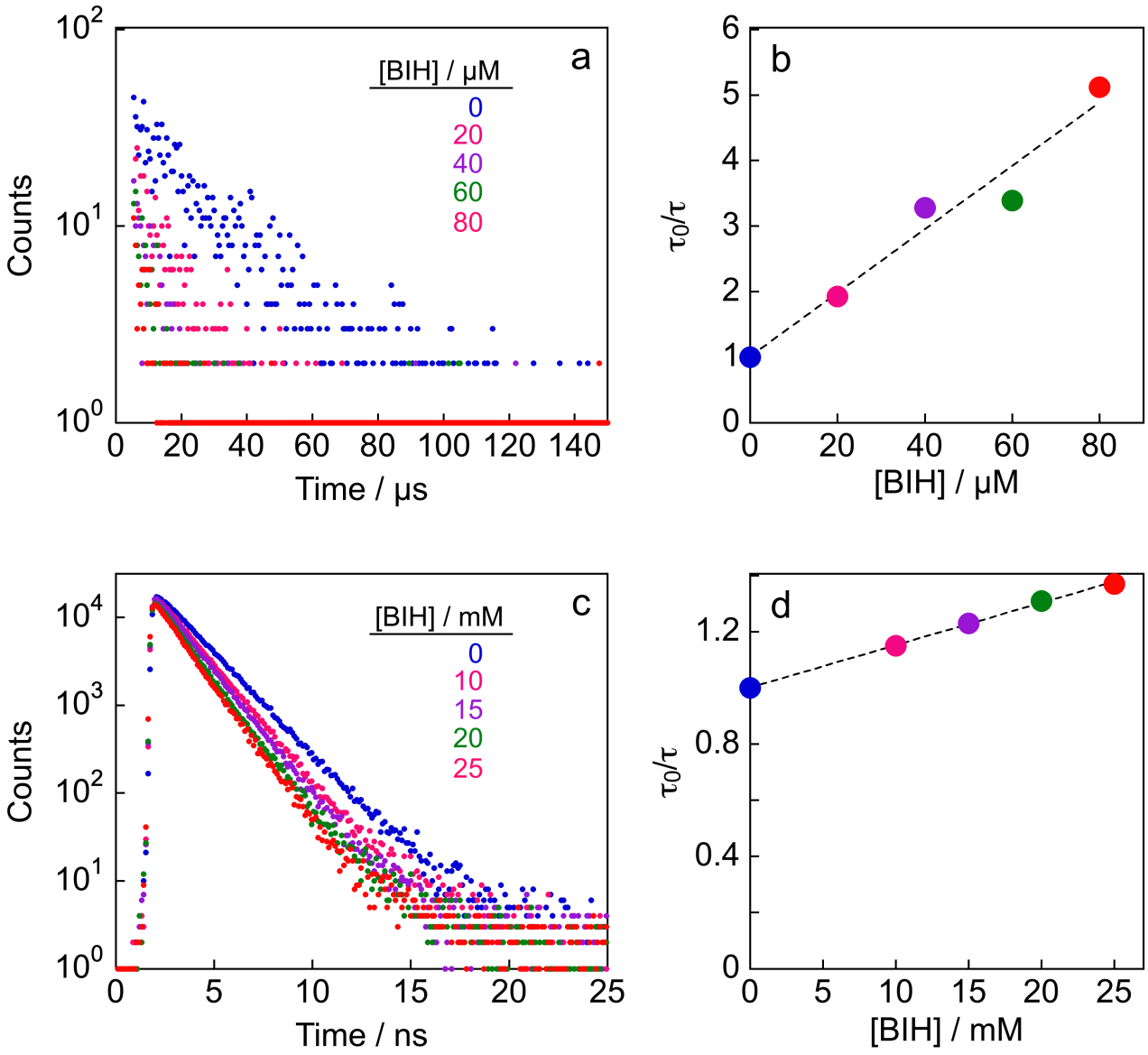

Figure S8. (a),(c) Emission intensity decays (λ_{em} = 530 nm) of **3DPAFIPN** in the presence of various concentrations of BIH and (b),(d) the corresponding Stern–Volmer plots. (a),(b) represents the quenching of TADF measured in Ar-saturated DMA–TEOA (1.5 M) upon λ_{ex} = 459 nm. (c),(d) represents the quenching of prompt fluorescence measured in air-equilibrated DMA–TEOA (1.5 M) upon λ_{ex} = 444 nm. Although both ^{1}**3DPAFIPN*** and ^{3}**3DPAFIPN*** are quenched by TEOA as well, for determining the quenching rate constants, we can assume that k_q^{TEOA}[TEOA] is constant and this value is included in τ_0 measured in DMA–TEOA (1.5 M). We selected this DMA–TEOA (1.5 M) solution because the properties of the solutions (such as viscosity) for measuring the quenching rate constants by BIH should be similar to those in the photocatalytic reactions.

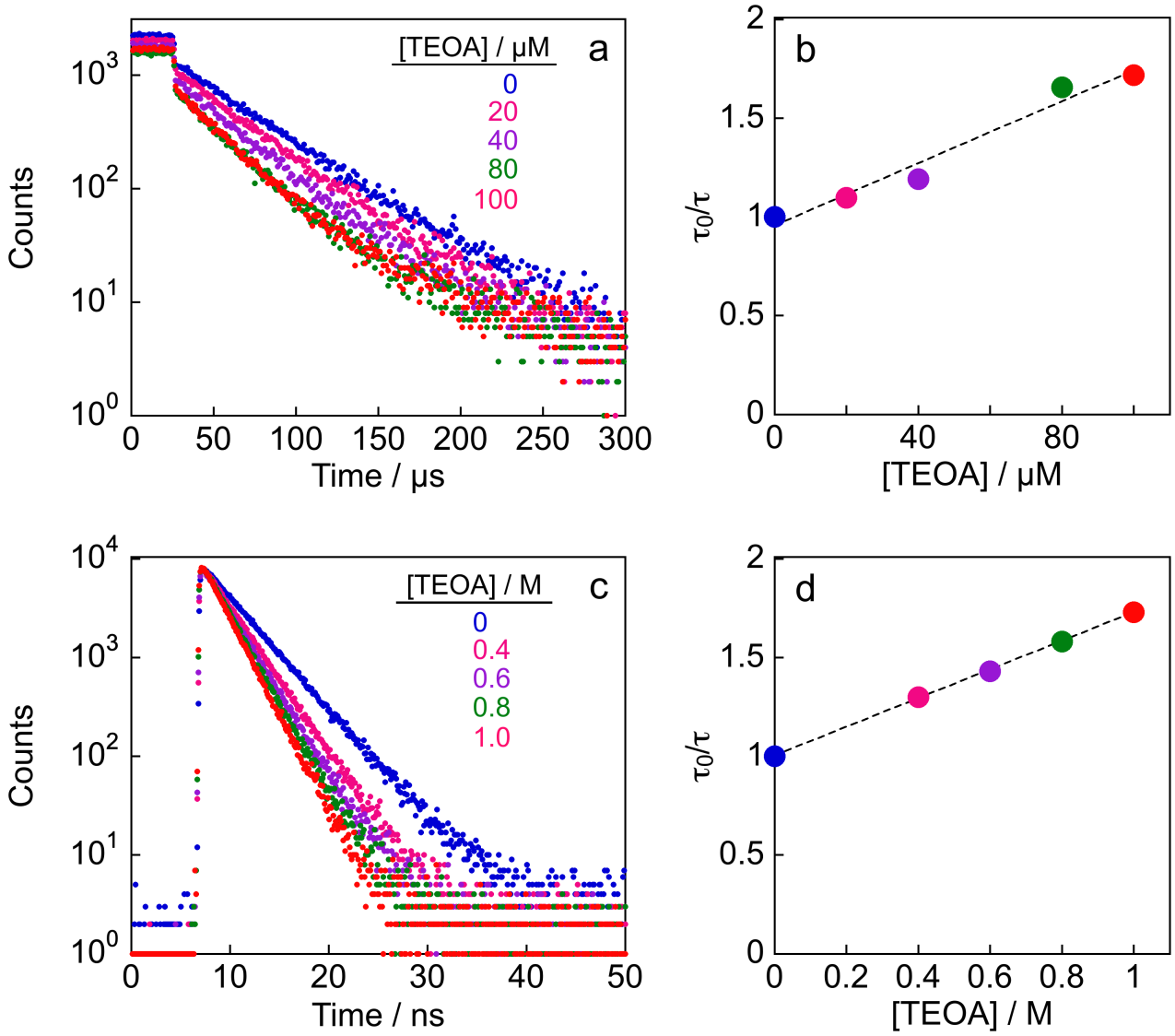

Figure S9. (a),(c) Emission intensity decays (λ_{em} = 530 nm) of **3DPAFIPN** in the presence of various concentrations of TEOA and (b),(d) the corresponding Stern–Volmer plots. (a),(b) represents the quenching of TADF measured in Ar-saturated DMA upon λ_{ex} = 459 nm. (c),(d) represents the quenching of prompt fluorescence measured in air-equilibrated DMA upon λ_{ex} = 444 nm.

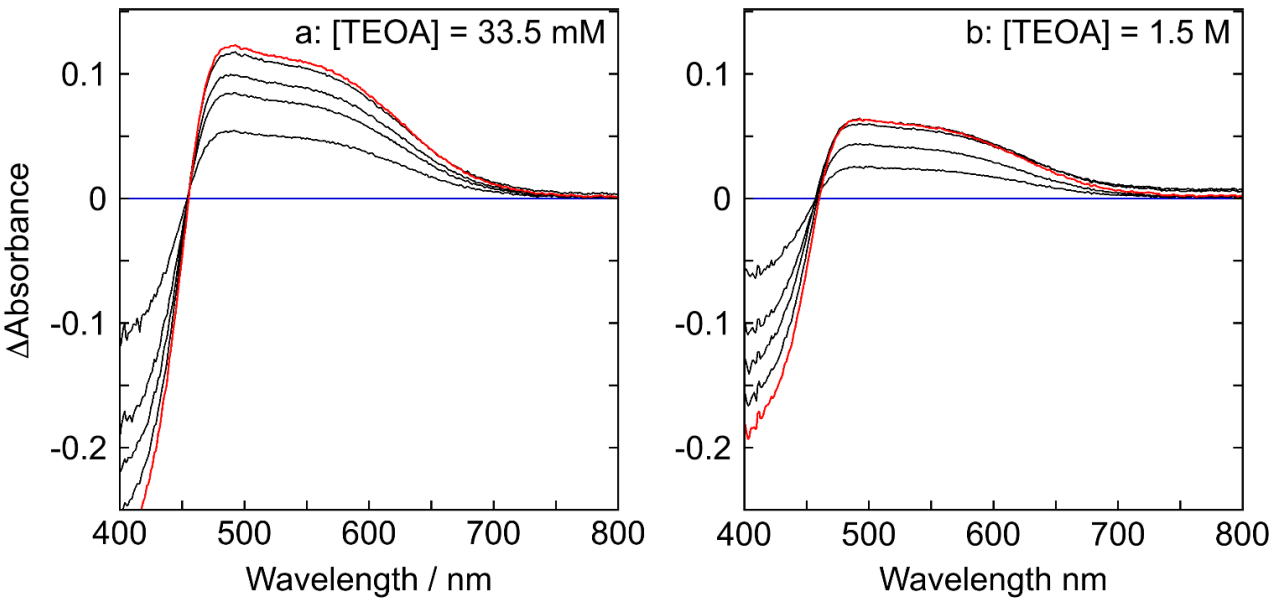

Figure S10. UV-vis differential absorption spectral change between post- and pre-irradiation spectra for 0-100 s at 20-s intervals: a CO_2-saturated DMA-TEOA (a: 33.5 mM; b: 1.5 M) solution containing **3DPAFIPN** (0.1 mM) were irradiated at 436-nm light. The blue and red lines represent the spectra of irradiation for 0 and 100 s, respectively. Light intensity was 1.0×10^{-8} Einstein·s^{-1}.

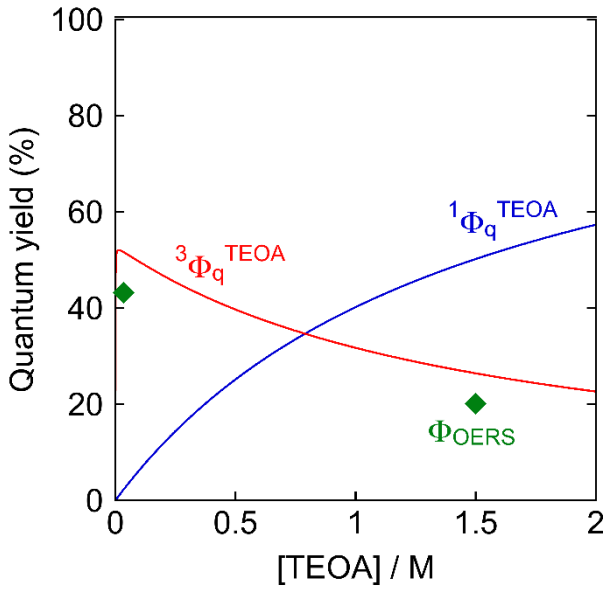

Figure S11. Observed quantum yields for the formation of **3DPAFIPN**$^{\cdot-}$ (◆) and calculated quantum yields for the reductive quenching of ^{1}**3DPAFIPN*** ($^1\Phi_q^{TEOA}$, blue line) and ^{3}**3DPAFIPN*** ($^3\Phi_q^{TEOA}$, red line) by TEOA as a function of the concentration of TEOA.

Kinetic analyses of photo-induced electron transfer processes (eqs. 2-7 are the same to the main text)

Although the following analyses show the case of **4DPAIPN**, the similar analyses can be applied to the case of **3DPAFIPN**.

In the absence of any quencher, the time course of the singlet and triplet excited states concentrations are described as eqs. S1 and S2.

$$\frac{d[^1\mathbf{4DPAIPN}^*]}{dt} = -(k_r + k_{nr} + k_{ISC})[^1\mathbf{4DPAIPN}^*] + k_{RISC}[^3\mathbf{4DPAIPN}^*] \quad (S1)$$

$$\frac{d[^3\mathbf{4DPAIPN}^*]}{dt} = k_{ISC}[^1\mathbf{4DPAIPN}^*] - k_{RISC}[^3\mathbf{4DPAIPN}^*] \quad (S2)$$

Since prompt fluorescence was not quenched at all in the presence of oxygen under air, whereas most of TADF was quenched, i.e. [^{3}**4DPAIPN***] ≈ 0 under air (see Figure 2), the reverse intersystem crossing process is negligible under air. Therefore, the prompt emission lifetime measured under air can be approximated by eq. S3.

$$\tau_{PF} = \frac{1}{k_r + k_{nr} + k_{ISC}} \quad (S3)$$

Phosphorescence from ^{3}4DPAIPN* was not observed. We can assume that the non-radiative decay of ^{3}**4DPAIPN*** is also negligible because it was reported as a much slower process compared to the RISC process to ^{1}**4DPAIPN***.[2] Therefore, by using eq. S3, the emission quantum yield measured under an Ar atmosphere is described as follows.

$$\begin{aligned}\Phi_{em}{}^{Ar} &= \Phi_{PF} + \Phi_{TADF} \\ &= \frac{k_r}{k_r + k_{nr} + k_{ISC}} + \frac{k_{ISC}}{k_r + k_{nr} + k_{ISC}} \times \frac{k_r}{k_r + k_{nr}} \\ &= \frac{k_r}{k_r + k_{nr}} \end{aligned} \quad (S4)$$

Using eqs. S3 and S4, k_r, k_{nr}, and k_{ISC} are described as below.

$$k_r = \frac{\Phi_{PF}}{\tau_{PF}} \quad (4)$$

$$k_{nr} = \frac{1 - (\Phi_{PF} + \Phi_{TADF})}{\Phi_{PF} + \Phi_{TADF}} k_r \quad (5)$$

$$k_{ISC} = \frac{1}{\tau_{PF}} - (k_r + k_{nr}) \quad (6)$$

In the time range exhibiting TADF, [^{3}**4DPAIPN***] >> [^{1}**4DPAIPN***] because k_{ISC} >> k_{RISC}, and, in addition, generation and decay processes of ^{1}**4DPAIPN*** are nearly balanced, resulting in a negligible time dependence of ^{1}**4DPAIPN*** (d[^{1}**4DPAIPN***]/dt ≈ 0). Therefore, the steady-state approximation of [^{1}**4DPAIPN***] can be established:[3] i.e., eq. S1 is transformed into eq. S5.

$$[^1\mathbf{4DPAIPN}^*] = \frac{k_{RISC}}{k_r + k_{nr} + k_{ISC}} [^3\mathbf{4DPAIPN}^*] \quad (S5)$$

From eqs. S2, S3 and S5, the following equations can be derived.

$$\frac{d[^3\mathbf{4DPAIPN}^*]}{dt} = -\frac{(k_r + k_{nr})k_{RISC}}{k_r + k_{nr} + k_{ISC}} [^3\mathbf{4DPAIPN}^*] \quad (S6)$$

$$\tau_{\mathrm{TADF}} \approx \frac{k_{\mathrm{r}} + k_{\mathrm{nr}} + k_{\mathrm{ISC}}}{(k_{\mathrm{r}} + k_{\mathrm{nr}})k_{\mathrm{RISC}}} = \frac{1}{(k_{\mathrm{r}} + k_{\mathrm{nr}})k_{\mathrm{RISC}}\tau_{\mathrm{PF}}} \tag{S7}$$

$$k_{\mathrm{RISC}} = \frac{1}{(k_{\mathrm{r}} + k_{\mathrm{nr}})\tau_{\mathrm{PF}}\tau_{\mathrm{TADF}}} \tag{7}$$

As described above, we can assume that the radiative and non-radiative decay of **^{3}4DPAIPN*** are negligible.[2] In addition, **^{1}4DPAIPN*** was quenched only by BIH whereas **^{3}4DPAIPN*** was quenched both by BIH and TEOA. Therefore, the concentration changes of S_1 and T_1 are expressed as eqs. 2 and 3.

$$\frac{d[\mathbf{^1\text{4DPAIPN}^*}]}{dt} = -\left(k_{\mathrm{r}} + k_{\mathrm{nr}} + k_{\mathrm{ISC}} + {}^1k_{\mathrm{q}}[\mathrm{BIH}]\right)[\mathbf{^1\text{4DPAIPN}^*}] + k_{\mathrm{RISC}}[\mathbf{^3\text{4DPAIPN}^*}] \tag{2}$$

$$\frac{d[\mathbf{^3\text{4DPAIPN}^*}]}{dt} = k_{\mathrm{ISC}}[\mathbf{^1\text{4DPAIPN}^*}] - (k_{\mathrm{RISC}} + {}^3k_{\mathrm{q}}^{\mathrm{BIH}}[\mathrm{BIH}] + {}^3k_{\mathrm{q}}^{\mathrm{TEOA}}[\mathrm{TEOA}])[\mathbf{^3\text{4DPAIPN}^*}] \tag{3}$$

$C_S(Q,t)$ and $C_T(Q,t)$ are functions of time and the concentrations of quenchers (Q: [BIH] and [TEOA]), representing the cumulative concentration of the singlet and triplet geminate ion pairs generated up to the time t. They do not represent the instantaneous concentration of the geminate ion pairs at a specific time, as the geminate ion pairs undergo subsequent processes such as cage escape and charge recombination. The time course of $C_S(Q,t)$ and $C_T(Q,t)$ are described as eqs. S8 and S9.

$$\frac{d}{dt}C_{\mathrm{S}}(Q,t) = {}^1k_{\mathrm{q}}^{\mathrm{BIH}}[\mathrm{BIH}][\mathbf{^1\text{4DPAIPN}^*}] \tag{S8}$$

$$\frac{d}{dt}C_{\mathrm{T}}(Q,t) = {}^3k_{\mathrm{q}}^{\mathrm{BIH}}[\mathrm{BIH}][\mathbf{^3\text{4DPAIPN}^*}] \tag{S9}$$

The particular solutions for $C_S(Q,t)$ and $C_T(Q,t)$ can be obtained by solving the differential equations (eqs. 2,3,S8, and S9) under the following initial conditions. The concentrations of BIH and TEOA can be assumed to be constant owing to their high concentrations in the initial stages of the photocatalytic reactions.

$$\left[\mathbf{^1\text{4DPAIPN}^*}\right]_{t=0} = C_0 \tag{S10}$$

$$[\mathbf{^3\text{4DPAIPN}^*}]_{t=0} = C_{\mathrm{S}}(Q,0) = C_{\mathrm{T}}(Q,0) = 0 \tag{S11}$$

where t=0 is defined as the time immediately after excitation of **4DPAIPN** to **^{1}4DPAIPN***, and C_0 represents the initial concentration of the generated **^{1}4DPAIPN***. Figure S12 shows the kinetic simulations of the reductive quenching processes (eq. 2, 3, S8, S9) with the initial conditions (eq. S10, S11) at BIH concentrations of 0.1 M and 0.01 M, using the determined rate constants of photophysical properties, i.e. k_r, k_{nr}, k_{ISC}, and k_{RISC} (eqs. 4-7), and the rate constants for reductive quenching (^1k_q, $^3k_q^{BIH}$, and $^3k_q^{TEOA}$) obtained by Stern-Volmer analyses. These simulations illustrate that the decrease in BIH concentration increases the quantum yield for the reductive quenching of **^{3}4DPAIPN*** by BIH ($^3\Phi_q^{BIH}$), while decreasing that of **^{1}4DPAIPN*** by BIH ($^1\Phi_q^{BIH}$). $^1\Phi_q^{BIH}$ and $^3\Phi_q^{BIH}$ are given by the asymptotic limits of $C_S(Q,t)$ and $C_T(Q,t)$ as t→∞ and can be expressed by the following equations (eqs. S12 and S13):

$${}^1\Phi_{\mathrm{q}}{}^{\mathrm{BIH}} = \frac{\lim_{t\to\infty} C_{\mathrm{S}}(Q,t)}{C_0}$$

$$= \frac{{}^{1}k_{\mathrm{q}}[\mathrm{BIH}]\left(k_{\mathrm{RISC}} + {}^{3}k_{\mathrm{q}}^{\mathrm{BIH}}[\mathrm{BIH}] + {}^{3}k_{\mathrm{q}}^{\mathrm{TEOA}}[\mathrm{TEOA}]\right)}{\left(k_{\mathrm{r}} + k_{\mathrm{nr}} + k_{\mathrm{ISC}} + {}^{1}k_{\mathrm{q}}[\mathrm{BIH}]\right)\left(k_{\mathrm{RISC}} + {}^{3}k_{\mathrm{q}}^{\mathrm{BIH}}[\mathrm{BIH}] + {}^{3}k_{\mathrm{q}}^{\mathrm{TEOA}}[\mathrm{TEOA}]\right) - k_{\mathrm{ISC}}k_{\mathrm{RISC}}} \quad \text{(S12)}$$

$${}^{3}\Phi_{\mathrm{q}}{}^{\mathrm{BIH}} = \frac{\lim_{t\to\infty} C_{\mathrm{T}}(Q,t)}{C_0}$$

$$= \frac{k_{\mathrm{ISC}}\,{}^{3}k_{\mathrm{q}}^{\mathrm{BIH}}[\mathrm{BIH}]}{\left(k_{\mathrm{r}} + k_{\mathrm{nr}} + k_{\mathrm{ISC}} + {}^{1}k_{\mathrm{q}}[\mathrm{BIH}]\right)\left(k_{\mathrm{RISC}} + {}^{3}k_{\mathrm{q}}^{\mathrm{BIH}}[\mathrm{BIH}] + {}^{3}k_{\mathrm{q}}^{\mathrm{TEOA}}[\mathrm{TEOA}]\right) - k_{\mathrm{ISC}}k_{\mathrm{RISC}}} \quad \text{(S13)}$$

As we described in the manuscript as well, the good agreement between the calculated quantum yields of the reductive quenching processes (${\Phi_{\mathrm{q}}}^{\mathrm{total}} = {}^{1}\Phi_{\mathrm{q}}{}^{\mathrm{BIH}} + {}^{3}\Phi_{\mathrm{q}}{}^{\mathrm{BIH}} + {}^{3}\Phi_{\mathrm{q}}{}^{\mathrm{TEOA}}$) based on the derived photophysical rate constants (8th column in Table 2) and the experimentally observed quenching fraction (η_{q}, 5th column) supports the validity of the rate constants which we determined.

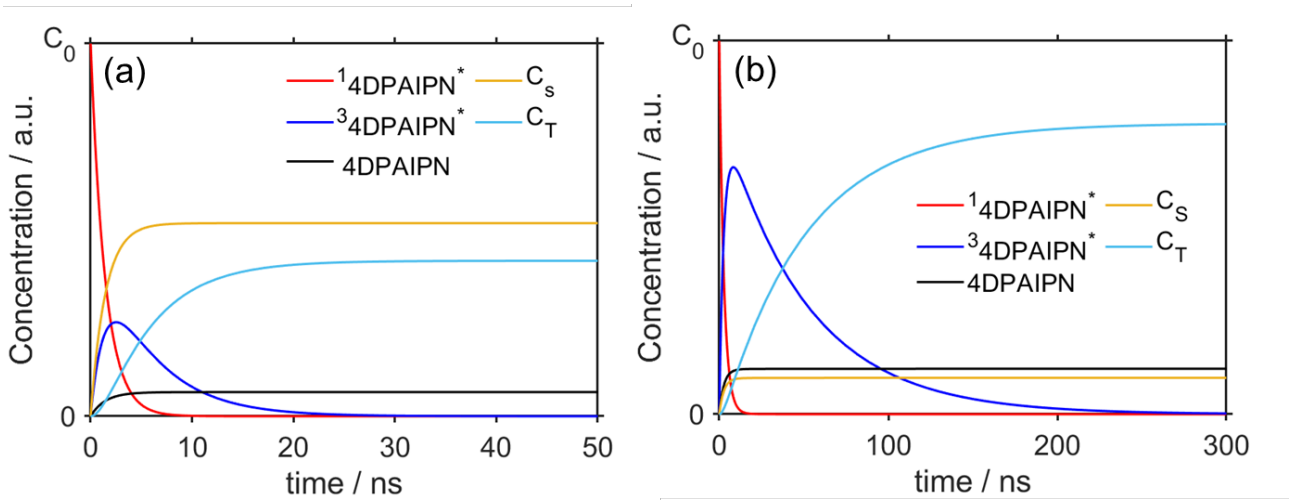

Figure S12. Kinetic simulations of the reductive quenching processes in the presence of (a) 0.1 M or (b) 0.01 M BIH.

Calculation of the escape yields from geminate ion pairs using **3DPAFIPN**

Because **3DPAFIPN** is reductively quenched both by TEOA and BIH, the calculation of escape yields during reductive quenching processes was conducted in two stages as follows:

(1) In the absence of BIH, the excited states of **3DPAFIPN** were quenched solely by TEOA. Using the observed quantum yields for the production of **3DPAFIPN**$^{\bullet-}$ (Φ_{OERS}) at two different concentrations of TEOA (33.5 mM and 1.5 M) and the calculated quantum yields for the reductive quenching ($^1\Phi_q^{TEOA}$ and $^3\Phi_q^{TEOA}$), the escape yields ($^1\eta_{esc}^{TEOA}$ and $^3\eta_{esc}^{TEOA}$) from ^{1}(**3DPAIPN**$^{\bullet-}\cdots$TEOA$^{\bullet+}$) and ^{3}(**3DPAIPN**$^{\bullet-}\cdots$TEOA$^{\bullet+}$) were estimated based on eq. S14 by least squares method.

$$\Phi_{OERS} = 2\times(^1\Phi_q^{TEOA}\times{}^1\eta_{esc}^{TEOA} + {}^3\Phi_q^{TEOA}\times{}^3\eta_{esc}^{TEOA}) \quad \text{(S14)}$$

(2) The escape yields from ^{1}(**3DPAIPN**$^{\bullet-}\cdots$BIH$^{\bullet+}$) and ^{3}(**3DPAIPN**$^{\bullet-}\cdots$BIH$^{\bullet+}$) were estimated in a similar manner using the observed quantum yields of **3DPAFIPN**$^{\bullet-}$ (Φ_{OERS}) at TEOA (1.5 M) and various concentrations of BIH, the escape yields determined at stage (1) ($^1\eta_{esc}^{TEOA}$ and $^3\eta_{esc}^{TEOA}$), and the calculated quantum yields for the reductive quenching ($^1\Phi_q^{BIH}$, $^3\Phi_q^{BIH}$, $^1\Phi_q^{TEOA}$, and $^3\Phi_q^{TEOA}$) based on eq. S15.

$$\Phi_{OERS} = 2\times(^1\Phi_q^{BIH}\times{}^1\eta_{esc}^{BIH} + {}^3\Phi_q^{BIH}\times{}^3\eta_{esc}^{BIH} + {}^1\Phi_q^{TEOA}\times{}^1\eta_{esc}^{TEOA} + {}^3\Phi_q^{TEOA}\times{}^3\eta_{esc}^{TEOA}) \quad \text{(S15)}$$

(1) Bassan, E.; Inoue, R.; Fabry, D.; Calogero, F.; Potenti, S.; Gualandi, A.; Cozzi, P. G.; Kamogawa, K.; Ceroni, P.; Tamaki, Y.; Ishitani, O. Visible-light driven photocatalytic CO_2 reduction promoted by organic photosensitizers and a Mn(i) catalyst. *Sustainable Energy Fuels* **2023**, *7*, 3454-3463.

(2) Song, Y.; Kim, Y.; Noh, Y.; Singh, V. K.; Behera, S. K.; Abudulimu, A.; Chung, K.; Wannemacher, R.; Gierschner, J.; Lüer, L.; Kwon, M. S., Organic Photocatalyst for ppm-Level Visible-Light-Driven Reversible Addition–Fragmentation Chain-Transfer (RAFT) Polymerization with Excellent Oxygen Tolerance. *Macromolecules* **2019,** *52*, 5538–5545.

(3) Tsuchiya, Y.; Diesing, S.; Bencheikh, F.; Wada, Y.; Dos Santos, P. L.; Kaji, H.; Zysman-Colman, E.; Samuel, I. D. W.; Adachi, C. Exact Solution of Kinetic Analysis for Thermally Activated Delayed Fluorescence Materials. *J. Phys. Chem. A*, **2021**, *125*, 8074-8089.